https://doi.org/10.5194/acp-2021-24
Preprint. Discussion started: 26 January 2021

Atmospheric Chemistry and Physics Discussions

Characterization of aerosol number size distributions and their effect on cloud properties at Syowa Station, Antarctica

Keiichiro Hara[1], Chiharu Nishita-Hara[2], Kazuo Osada[3], Masanori Yabuki[4], and Takashi Yamanouchi[5]

[1] Department of Earth System Science, Faculty of Science, Fukuoka University, Fukuoka, 814-0180, Japan
[2] Fukuoka Institute for Atmospheric Environment and Health, Fukuoka University, Fukuoka, 814-0180, Japan
[3] Graduate School of Environmental Studies, Nagoya University, Nagoya, 464-8601, Japan
[4] Research Institute for Sustainable Humanosphere, Kyoto University, Kyoto, 611-0011, Japan
[5] National Institute of Polar Research, Tokyo, 190-0014, Japan

Correspondence to: Keiichiro Hara (harakei@fukuoka-u.ac.jp)

Abstract. We took aerosol measurements at Syowa Station, Antarctica to characterize the aerosol number–size distribution and other aerosol physicochemical properties. Four modal structures (i.e., mono-, bi-, tri-, and quad-modal) were identified in aerosol size distributions during measurements. Particularly, quad-modal structures were associated closely with new particle formation (NPF). To elucidate where NPF proceeds in the Antarctic, we compared the aerosol size distributions and modal structure to air mass origins computed using backward trajectory analysis. Results of this comparison imply that NPF occurred in free troposphere during spring and autumn, and in the free troposphere and boundary layer during summer. Photochemical gaseous products, coupled with UV radiation, play an important role in NPF, even in the Antarctic troposphere. With the appearance of the ozone hole in the Antarctic stratosphere, more UV radiation can enhance atmospheric chemistry, even near the surface in the Antarctic. However, linkage among tropospheric aerosols in the Antarctic, ozone hole, and UV enhancement is unknown. Results demonstrated that NPF started in the Antarctic free troposphere already in the end-August – early September by UV enhancement resulting from the ozone hole. Then, aerosol particles supplied from NPF during spring grow gradually by vapor condensation, suggesting modification of aerosol properties such as number concentrations and size distributions in the Antarctic troposphere during summer. Here, we assess the hypothesis that UV enhancement in the upper troposphere by the Antarctic ozone hole modifies the aerosol population, aerosol size distribution, cloud condensation nuclei capabilities, and cloud properties in Antarctic regions during summer.

1 Introduction

The Antarctic is isolated from human activities occurring in the mid-latitudes. In spite of the slight amount of human activity in the Antarctic, such as research activities at each station and tourism mostly in the Antarctic Peninsula during summer, the source strength of anthropogenic species (e.g. black carbon from combustion processes) is negligible in the Antarctic circle at the moment (e.g., Weller et al., 2013; Hara et al., 2019). Consequently, aerosol measurements in the Antarctic have been taken to ascertain aerosol physicochemical properties, atmospheric chemistry, and their effects on climate change in Earth's background conditions (i.e. cleanest and pristine conditions).

Despite the cleanest conditions prevailing in the Antarctic, concentrations of condensation nuclei (CN) show clear seasonal variations with maximum in summer and minimum in winter (Gras et al., 1993; Hara et al., 2011a; Weller et al., 2011). This seasonal variation relates to supply and deposition processes. In addition to primary aerosol emissions such as sea-salt aerosols from sea-surface and sea-ice regions (e.g., Hara et al., 2020), atmospheric aerosol formation (i.e. new particle formation, NPF) is important to supply atmospheric aerosols (Kulmala et al., 2013; Kerminen et al., 2018) and to affect climate through indirect processes (Asmi et al., 2010; Dall'Osto et al., 2017). To elucidate and discuss NPF, particle growth,

https://doi.org/10.5194/acp-2021-24
Preprint. Discussion started: 26 January 2021

and aerosol properties in sub-micrometer ranges, aerosol number size distributions have been measured even in the Antarctic using scanning mobility particle sizer (SMPS; Koponen et al., 2003; Virkkula et al., 2007; Asmi et al., 2010; Hara et al., 2011b; Kyrö et al., 2013; Järvinen et al., 2013; Weller et al., 2015; Kim et al., 2019; Jang et al., 2019; Lachlan-Cope et al., 2020) and similar instrument (Ito, 1993). Seasonal features of aerosol number concentrations are associated with NPF, emissions of aerosol precursors from oceanic bioactivity, and photochemical processes (Koponen et al., 2003; Virkkula et al., 2007; Asmi et al., 2010; Hara et al., 2011a; Kyrö et al., 2013; Järvinen et al., 2013; Fiebig et al., 2014; Weller et al., 2015; Humphries et al., 2016). Actually, NPF was observed along the Antarctic coasts during summer at the boundary layer (Koponen et al., 2003; Virkkula et al., 2007; Asmi et al., 2010; Kyrö et al., 2013; Weller et al., 2015; Kim et al., 2019; Jang et al., 2019; Lachlan-Cope et al., 2020) and in the free troposphere (Hara et al., 2010; Humphries et al., 2016; Lachlan-Cope et al., 2020). Additionally, earlier works (Hara et al., 2011a; Järvinen et al., 2013; Kim et al., 2019) have emphasized that NPF occurs as early as September in the Antarctic. However, most earlier works have specifically examined summer NPF in the Antarctic (Koponen et al., 2003; Virkkula et al., 2007; Asmi et al., 2010; Kyrö et al., 2013; Weller et al., 2015; Humphries et al., 2016).

Earlier works have emphasized examination of the following condensable vapors (i.e. aerosol precursors) for NPF and particle growth: H_2SO_4, CH_3SO_3H, HIO_3, amines, and other organics with low vapor pressure (Yu et al., 2012; Kulmala et al., 2013; Kyrö et al., 2013; Weller et al., 2015; Simplä et al., 2016; Jen et al., 2016; Shen et al., 2019; Burrell et al., 2019). In Antarctic regions, biogenic activity in the ocean around the sea–ice margin is crucially important for emissions of precursors of the condensable vapors (e.g., Minikin et al., 1998; Weller et al., 2015; Enami et al., 2017; Jang et al., 2019). Additionally, aerosol precursors can be emitted because of snowpack chemistry (Roscoe et al., 2015) and melt ponds on the Antarctic continent (Kyrö et al., 2013). Condensable vapors for NPF and aerosol growth are formed through photochemical reactions with atmospheric oxidants such as OH, O_3, and BrO (Read et al., 2008). They relate to UV radiation (Matsumi et al., 2002; Matsumi and Kawasaki, 2003). Appearance of the ozone hole in the Antarctic stratosphere during September–November (Hoppel et al., 2005) is expected to enhance UV radiation and atmospheric oxidation potential in the troposphere (Jones et al., 2003). Nevertheless, the effects on aerosols in the Antarctic troposphere have not been elucidated sufficiently. Because of the low aerosol number concentrations, direct effects of aerosol radiative forcing are negligible in the Antarctic (Bodhaine, 1995). After aerosol activation to cloud condensation nuclei (CCN), indirect effects might affect the atmospheric radiation budget and climate (Bromwich et al., 2012). With the present study, we are striving to understand the occurrence of NPF in the Antarctic, linkage among NPF, the ozone hole, and cloud properties in the Antarctic coast (around Syowa Station).

2 Experiments and analysis

2.1 Aerosol measurements at Syowa station, Antarctica

Aerosol measurements were taken during the 45th–47th Japanese Antarctic Research Expedition (2004–2006) at Syowa Station, Antarctica (69.0 °S, 39.0 °E), located on East Ongul Island in Lützow Holm Bay. Size distributions of ultrafine particles (diameter (D_p): 5 – 168 nm) were measured using SMPS (3936-N-25; TSI Inc.) during February 2004 – December 2006. A condensation particle counter (CPC) was used (3025A; TSI Inc.) to take SMPS measurements. Each scan for SMPS measurements took 5 min. In addition, an optical particle counter (OPC: KC22B; Rion Co. Ltd.) was used for measurements of size distributions of aerosols with size of D_p >0.08, >0.1, >0.2, 0.3, and >0.5 μm during January 2005 – December 2006. In OPC measurements, number concentrations were recorded every minute. SMPS and OPC were operated at room temperature of ca. 20 °C in the clean air observatory located at the windward side ca. 400 m distant from the main area of the station, where a diesel generator was operated. When winds came from the main area, local contamination might have

https://doi.org/10.5194/acp-2021-24
Preprint. Discussion started: 26 January 2021

Atmospheric Chemistry and Physics Discussions

occurred. Before analysis and discussion, locally contaminated data were screened using condensation nuclei concentrations (measured as aerosol monitoring at Syowa Station) and wind data (provided by the Japanese Meteorological Agency). Data screening procedures and criteria were identical to those described in earlier reports (Hara et al., 2011b, 2019). After screening of locally contaminated data, daily mean aerosol number concentrations and size distributions were calculated for data analysis. Aerosol sampling for chemical analysis was made using a two-stage mid-volume impactor and a back-up filter. Water soluble aerosol constituents were determined using ion chromatography. Details of aerosol sampling and chemical analysis were given in reports of our earlier work (Hara et al., 2004, 2018).

2.2 Data analysis

2.2.1 Estimation of coagulation sink and condensation sink

Nano-size aerosol particles are removed rapidly through coagulation. To elucidate the removal speed by coagulation, coagulation sink (Coag.S) was calculated using the following equation (Kulmala et al., 2001).

$$\text{Coag. S} = \sum_j K_{ij} N_j \quad (1)$$

Therein, K_{ij} and N_j respectively represent the coagulation coefficient in the transitional regime and the number concentrations of the size bin of j.

Condensation sink (Cond.S) was calculated to elucidate the removal speed of condensable vapours by condensation on aerosol particles using the following equation (Kulmala et al., 2001).

$$Cond.S = 4\pi D \int_0^\infty r\beta_M(r)\ n(r)dr = \sum_i \beta_M r_i N_i \quad (2),$$

where r and β_M indicate particle radius and the transitional correction factor. Details of calculation procedures were presented in an earlier report (Kulmala et al., 2001).

2.2.2 Estimation of the nucleation rate of aerosol particles

The nucleation rate of aerosol particles (D_p = 5 nm: J_5) was estimated as elucidating NPF and particle growth in the Antarctic troposphere. Number concentrations (N) of nano-size aerosol particles in each size bin depend on (1) growth from the smaller size by vapor condensation, (2) coagulation loss, and (3) growth to larger size by condensation. To calculate J_5, three size bins based on particles were used: D_p 1–5 nm, 5–10 nm, and 10–20 nm (Fig. 1). The change of the number concentrations in each size bin can be given by the following equation using *Coag.S* and the condensation growth rate (*Cond*).

$$\frac{dN_{1-5}}{dt} = J_1 - Coag.S_{1-5}N_{1-5} - Cond_{1-5}N_{1-5} \quad (3)$$

$$\frac{dN_{5-10}}{dt} = J_5 - Coag.S_{5-10}N_{5-10} - Cond_{5-10}N_{5-10} \quad (4)$$

$$\frac{dN_{10-20}}{dt} = J_{10} - Coag.S_{10-20}N_{10-20} - Cond_{10-20}N_{10-20} \quad (5)$$

In this procedure, the aerosol growth rate ($Cond_iN_i$) in i bin corresponds to J_{i+1}. Furthermore, we assumed that the daily mean aerosol size distributions can be approximated as an equilibrium condition, i.e. $dN_{5-10}/dt \approx 0$ and $dN_{10-20}/dt \approx 0$. Therefore, J_5

https://doi.org/10.5194/acp-2021-24
Preprint. Discussion started: 26 January 2021

Atmospheric Chemistry and Physics Discussions

is obtainable from $Coag.S_{5–10}N_{5–10}$ and $Coag.S_{10–20}N_{10–20}$. It is noteworthy that the estimated J_5 is the lower limit value, especially in the occurrence of strong NPF and particle growth by condensation. Also, primary emissions of ultrafine aerosol particles can engender false estimation of J_5. Sea-salt particles were dominant even among ultrafine aerosol particles under storm conditions that prevailed during winter–spring at Syowa Station (Hara et al., 2011b). Indeed, high J_5 was identified occasionally in the high contribution of sea-salt particles during winter.

2.2.3 Lognormal fitting of aerosol size distributions

Daily mean aerosol size distributions were approximated by a lognormal function, which is given by the following equation.

$$\frac{dN}{dlogD_p} = \sum_{i=1}^{n} \frac{N_i}{\sqrt{2\pi} log\sigma_i} exp\left[-\frac{(logD_p - logD_{p,i})}{2log^2\sigma_i}\right] \quad (6)$$

In equation (9), D_p, n, $D_{p,\,i}$, σ_i, and N_i respectively denote the particle diameter, mode number (n = 1–4), modal mean diameter in mode i, modal standard deviation in mode i, and the aerosol number concentrations in mode i. Lognormal fitting was performed using the nls.lm function of minpack.lm library of R (R interface to the Levenberg–Marquardt nonlinear least-squares algorithm found in MINPACK). To avoid unrealistic lognormal fitting, we set the following restrictions: (1) N_i > 1% of total particle concentrations, (2)$1.2 \le \sigma_i \le 2.2$, and (3) $1.3\ D_{p,\,i} < D_{p,\,i+1}$. The daily mean aerosol size distributions (D_p = 5–168 nm: SMPS only) were approximated by lognormal functions in 2004. The size distributions (D_p = 5–300 nm: SMPS + OPC) were analyzed by lognormal fitting in 2005–2006. For this study, we defined each mode based on the particle size range as follows: fresh nucleation mode (D_p <10 nm), aged nucleation mode (D_p = 10–25 nm), first Aitken mode (D_p = 25–50 nm), second Aitken mode (D_p = 50–100 nm), and accumulation mode (D_p >100 nm).

2.3 Backward trajectory analysis

The 120-hr (5-day) backward trajectory was computed using the NOAA-HYSPLIT model (https://ready.arl.noaa.gov/HYSPLIT.php) with the NCEP meteorological dataset (reanalysis) in model vertical velocity mode. The initial point was at 500 m above ground level over Syowa Station, Antarctica. For this study, we use the following criteria to divide each air mass origin: marine, <66 °S; coastal, 66–75°S; Antarctic-continental, >75 °S; boundary layer (BL), <1500 m; and free troposphere (FT), >1500 m. Then, the time passing in each area such as marine BL (MBL), coastal BL, continental BL, continental FT, coastal FT, and marine FT (MFT) was counted for each backward trajectory. Areas with air masses staying for the longest times in the 5-day backward trajectory were classified into air mass origins.

3 Results and Discussion

3.1 Aerosol size distributions

Figure 2 presents examples of number size distributions of aerosol particles observed at Syowa Station. Our measurements show size distributions of ultrafine aerosol particles with mono-, bi-, tri-, and quad-modal structures. To characterize the aerosol size distributions, we compare the modal size in each mode (Fig. 3). In mono-modal distributions, the modal size ranged mostly in 40–105 nm. In bi-modal structures, the respective modal sizes in first and second modes were distributed in 20–40 nm and 60–135 nm. In tri-modal distributions, first–third modal sizes appeared in 8–20, 20–63, and 65–135 nm, respectively. Quad-modal structure had respective modal sizes of 7–13, 14–30, 30–65, and 70–140 nm. Because the smallest mode appeared with diameter smaller than 20 nm, occasionally smaller than 10 nm, in tri-modal and quad-modal structures,

https://doi.org/10.5194/acp-2021-24
Preprint. Discussion started: 26 January 2021


Atmospheric Chemistry and Physics Discussions

aerosol size distributions with tri-modal and quad-modal structures might be associated with NPF and growth by vapor condensation.

Figure 4 shows the seasonal variation of abundance of modal structures at Syowa Station during our measurements. Mono-modal and bi-modal structures were dominant in May–August. Mono-modal structures were identified under the strong winds and the storm conditions with blowing snow (Hara et al., 2011b). Bi-modal structures were found through the year. High abundance of tri-modal structure was observed in September–April. Particularly, abundance of tri-modal structures exceeded 50% in January–March. Surprisingly, tri-modal structures were identified even in winter (May–August) in spite of lower solar radiation (i.e. polar night). Modal sizes in the smallest mode of tri-modal structure were larger in winter than those in spring–summer (details will be presented in a later section). It is noteworthy that the quad-modal structure was found not only in December–February, but also in August–November and March–April. Considering the modal size in the smallest mode of quad-modal distributions, NPF might proceed in August–April in the Antarctic. Indeed, CN concentrations started to increase in August, with high concentrations in October–February at the coastal stations (e.g., Hara et al., 2011a, Weller et al., 2011; Asmi et al., 2013).

3.2 Relation between modal structures and air mass history

Annual cycles of air mass origins in each modal structure using 120-hr backward trajectory analysis are shown in Figure 5 for comparison between the modal structure and air mass history. Regarding general features of air mass origins in February 2004 – December 2006, coastal boundary layer (BL) was dominant in summer (Fig. 5a), whereas abundance of continental free troposphere (FT) increased during winter. The seasonal cycles of air mass origins in 2004 – 2006 showed good agreement with long-term analysis of air mass origins at Syowa during 2005–2016 (Hara et al., 2019).

Seasonal features of air mass origins in mono-modal distributions (Fig. 5b) were similar to the general features (Fig. 5a), although the abundance of coastal FT was slightly higher in August and October. Considering that mono-modal structures corresponded mostly to storm conditions and strong winds during winter–spring (Hara et al., 2010, 2011b, 2020), the appearance of mono-modal structure were associated with primary emissions of sea-salt aerosols from the snow surface on sea-ice by strong winds rather than air mass history (i.e. transport pathway).

Similarly, seasonal features of air mass origins in bi-modal structure (Fig. 5c) resembled the general features. In general, bi-modal structures were recognized as well-aged distributions by condensation growth, coagulation, cloud processes, and so on. Therefore, the appearance of bi-modal structures might be compared only slightly to air mass origins classified by 120-hr backward trajectory analysis.

In the tri-modal structure (Fig. 5d), the abundance of continental FT and coastal FT increased in spring, compared to the general features (Fig. 5a). Similarly to bi-modal structures, the appearance of some tri-modal structures, particularly with larger modal size (e.g., D_p>20 nm) in the smallest mode needed aging processes for a longer time. Consequently, seasonal variations of air mass origins in tri-modal structures were similar to general features, although sum of abundance of continental FT and coastal FT exceeded 50–60 % in August – October. This abundance was slightly higher than that of the general features.

Unlike the features in mono-modal, bi-modal, and tri-modal structures, continental FT and coastal FT were the most abundant air mass origins in quad-modal structures during spring and autumn (Fig. 5e). In general, features of air mass origins (Fig. 5a), marine BL and coastal BL showed an important contribution during spring and autumn. Nevertheless,

https://doi.org/10.5194/acp-2021-24
Preprint. Discussion started: 26 January 2021

Atmospheric Chemistry and Physics Discussions

quad-modal structures in spring and autumn were identified only in the air mass from continental FT and coastal FT. This feature implies strongly that NPF proceeded in FT during spring and autumn in the Antarctic. In contrast to the high contributions of continental FT and coastal FT during spring and autumn, quad-modal structures were observed also in marine BL and coastal BL during summer. Therefore, NPF might occur also in marine BL and coastal BL during summer, as reported from results of earlier works (Weller et al., 2011; Asmi et al., 2013; Lachlan-Cope et al., 2020). It is noteworthy that the abundance of continental FT and coastal FT during summer decreased remarkably, even in general features (Fig. 5a). Furthermore, the quad-modal structure was observed in continental FT and coastal FT in December (summer). CN enhancement by NPF and growth was observed in the lower free troposphere over Syowa Station during summer (Hara et al., 2011a). Therefore, the difference of contributable air mass origins in quad-modal structures between spring–autumn and summer might reflect not only the locations of NPF occurrence but also seasonal features of general air mass origins (Fig. 5a). Consequently, NPF might occur in FT during spring and autumn and in BL and FT during summer.

3.3 Seasonal variations of aerosol physicochemical properties

Figure 6 depicts seasonal variations of all of the following: (a) concentrations of major aerosol constituents in D_p <200 nm; (b) modal sizes and number concentrations of each mode; (c) aerosol number concentrations of fresh nucleation mode (D_p = 5–10 nm); (d) coagulation sinks and condensation sinks; (e) nucleation rates of aerosol particles with D_p = 5 nm (J_5); (f) extent of the Antarctic ozone hole; and (g) UV radiation near the surface at Syowa Station. Major water-soluble aerosol constituents of less than D_p = 200 nm are $CH_3SO_3^-$ and non-sea-salt (nss) SO_4^{2-} in summer and sea-salt (e.g., Na^+) in winter (Fig. 6a). The $CH_3SO_3^-$ concentrations, which start increasing at the end of August–September, show maximum concentrations in February–March at Syowa Station. Seasonal variation of $CH_3SO_3^-$ concentrations implies that oceanic bioactivity and atmospheric photochemistry contribute to the maintenance of aerosol systems in September – early April because precursors of $CH_3SO_3^-$ (e.g., dimethylsulfide, DMS) derive from oceanic bioactivity (Minikin et al., 1998).

Our measurements show size distributions of ultrafine aerosol particles with mono-, bi-, tri-, and quad-modal structures (Fig. 2). The presence of tri-modal and quad-modal structures during spring–autumn suggests the frequent occurrence of NPF and growth in the atmosphere. Indeed, fresh-nucleation and aged-nucleation modes (D_p: <10 nm and 10–25 nm) appeared often in spring–summer (Fig. 6b). Particularly, fresh nucleation mode appeared only in end-August – early October and February–March. Furthermore, the modal sizes increased gradually from fresh nucleation mode to first Aitken mode (D_p = 25–50 nm) in September–December. Such a gradual size shift implies that aerosol particles derived from NPF grew by the condensation of condensable vapors such as H_2SO_4.

Aerosol number concentrations of D_p = 5–10 nm ($N_{5–10}$) show three maxima in September–October, December, and February–March (Fig. 6c) when tri-modal and quad-modal structures appeared frequently. These periods respectively correspond to the appearance of the ozone hole (September–October marked by grey-shaded bands), the maximum of solar radiation (summer solstice marked by blue-shaded bands), and the minimum of the sea ice extent (February–March marked by green-shaded bands). In general, $N_{5–10}$ was controlled by (1) NPF and growth from smaller size (ca. 1 nm), (2) coagulation loss, and (3) particle growth to larger sizes by vapor condensation. Additionally, J_5 showed three maxima similar to $N_{5–10}$ variation (Fig. 6e). Although high J_5 was observed often during May – August, this phenomenon might derive from dispersion of sea-salt aerosols from sea-ice areas by strong winds (Hara et al., 2011b). Therefore, high J_5 in the spring and summer are expected to be related to NPF.

The high J_5 and $N_{5–10}$ in December and February–March are explainable by photochemical reactions, which form condensable vapors, and by the source strength of aerosol precursors released from oceanic bioactivity near the sea–ice

https://doi.org/10.5194/acp-2021-24
Preprint. Discussion started: 26 January 2021

Atmospheric Chemistry and Physics Discussions

margin. By contrast, the sea–ice extent showed a maximum in spring (September – November, Fig. 6f). Consequently, other factors affecting the likelihood of high J_5 and $N_{5–10}$ in spring should be considered. To elucidate the presence of fresh nucleation mode in spring, the location at which NPF occurred in the Antarctic region must be discussed. Air masses having quad-modal structures with fresh nucleation mode originated mostly from the upper free troposphere over the Antarctic continent (Supplementary, Fig. S1). *Coag.S* of D_p = 5 nm aerosol particles increased gradually from 2×10^{-6} s^{-1} to 10^{-5} s^{-1} during September–December (Fig. 6d). From *Coag.S*, we estimated the e-folding time of the particles (D_p = 5 nm) by coagulation loss to 3.9–5.8 days in early September and 1.2–1.4 days in December (Supplementary, Fig. S2). This finding implies that the particles in the fresh nucleation mode observed at Syowa had too short a lifetime to be supplied by long-range transport from the mid-latitudes via the free troposphere. Therefore, NPF should start in the Antarctic free troposphere already by end-August.

Generally speaking, NPF is more likely to occur under conditions with (1) lower number concentrations of preexisting particles, (2) higher concentrations of condensable vapors, and (3) presence of sufficient photochemical oxidants such as OH. Because of low aerosol number concentrations in the Antarctic free troposphere (Hara et al., 2011a), NPF can proceed preferentially in the free troposphere if condensable vapor is present. Considering the important contributions of $CH_3SO_3^-$ and nss-SO_4^{2-} in ultrafine particles (Fig. 6a), H_2SO_4 and CH_3SO_3H converted from DMS by reactions with the atmospheric oxidants are regarded as plausible condensable vapors. Because of the winter maximum of DMS observed on the Antarctic plateau (Preunkert et al., 2008), aerosol precursors such as DMS are likely to be available in the Antarctic free troposphere during winter–spring. Sufficient photochemical oxidants such as OH and UV radiation are necessary for the conversion of condensable vapors. Atmospheric OH is producible by the following reactions under conditions with UV radiation ($\lambda \leq 310$ nm) (Matusmi et al., 2002; Matsumi and Kawasaki, 2003).

$$O_3 + h\nu \rightarrow O_2 + {}^1D \qquad \text{(R1)}$$
$$H_2O + {}^1D \rightarrow 2OH \qquad \text{(R2)}$$

Polar sunrise in the upper free troposphere occurs earlier than near the surface. Additionally, the appearance of the ozone hole enhances UV radiation, even in the troposphere during September–November (Figs. 6f–g). More noteworthy is the higher UV in October–November than in December near the surface at Syowa. Considering the greater amount of UV radiation in the upper troposphere during September – November, the appearance of the ozone hole might enhance the formation of photochemical oxidants (e.g., OH) and condensable vapors, which then engender NPF in the upper troposphere (Figs. 6b–c). Although aerosol particles in fresh nucleation mode can be coagulated efficiently onto pre-existing particles, the e-folding time of aerosol particles (D_p = 10, 20, and 30 nm) by coagulation was estimated respectively as 10–15 days, 10–30 days, and 11–48 days (Fig. 6d and Supplementary Fig. S2). These values were estimated based on aerosol size distributions measured near the surface. Therefore, longer e-folding time is expected in the free troposphere with lower concentrations of preexisting particles and condensable vapors (Hara et al., 2011a). Consequently, aerosol particles can be grown gradually through condensation of condensable vapors in the Antarctic troposphere once new particles grow to the aged nucleated particles (D_p >10 nm). Finally, UV enhancement in the upper troposphere by the ozone hole might modify the aerosol population and size distributions in the Antarctic troposphere during spring–summer. Therefore, aerosol properties in the Antarctic troposphere during spring – summer are not “pristine” but under the Anthropocene conditions, although the Antarctic troposphere remains the cleanest on the earth.

https://doi.org/10.5194/acp-2021-24
Preprint. Discussion started: 26 January 2021

Atmospheric Chemistry and Physics Discussions

3.4 CCN potential and cloud amount during summer

Gradual change of modal sizes in fresh nucleation mode and first Aitken mode were observed during spring–summer (Fig. 6b). When aerosol particles derived from spring NPF during end-August – November grow to critical diameter, the aerosol particles can act as CCN. The critical diameter measured at Aboa Station was ca. 50 nm (Asmi et al., 2010). Gradual particle growth in the aged-nucleation and first Aitken modes (Fig. 6b) suggest that spring NPF and growth are linked to cloud properties during summer. Here, we attempt to estimate the contribution of aerosols derived from spring NPF to act as CCN in November–January based on the following assumptions: aerosol particles supplied from spring NPF were grown to aged-nucleation and first Aitken modes. For this estimation, the contribution to CCN (R_{CCN}) was defined as the ratio of the aerosol number concentrations of D_p >50 nm in aged-nucleation and first Aitken modes ($N_{D>50}$) to the total aerosol number concentrations in D_p >50 nm (total-$N_{D>50}$, Fig. 7). The value of R_{CCN} was estimated using the following equation.

$$R_{CCN}(\%) = \frac{N_{D>50}}{total - N_{D>50}} \times 100 \quad (7)$$

Results show that R_{CCN} in the continental free troposphere was significantly greater than that at the coastal boundary layer (Fig. 8). Although NPF can proceed during summer, the smaller mode was distributed in D_p <30 nm by summer NPF and growth. Therefore, aerosol particles supplied from summer NPF in the boundary layer were not grown sufficiently to the critical diameter by condensation. We infer that aerosol enhancement by spring NPF might modify not only aerosol size distributions but also CCN ability in summer.

Trends of cloud amounts at Syowa Station were examined to assess impact of spring NPF enhanced by appearance of O_3 hole on CCN ability during summer. Figure 9 depicts variations of cloud amounts in December and January since 1969. Although no increasing trend was identified for air temperature or water vapor concentrations related to the cloud amount, a marked increasing trend with p values lower than 0.01 was found only for December and January during 1969–2012. Particularly, the cloud amount at Syowa Station was significantly higher after the appearance of the O_3 hole (Fig. 9b, and Fig. S3). Consequently, the cloud amount trend during summer might result from spring NPF enhanced by O_3 hole appearance. Because of the conformable relation between the cloud amount and radiative fluxes (Yamanouchi et al., 2007), UV enhancement by the O_3 hole can affect atmospheric radiation budgets by aerosol/cloud properties in the Antarctic during summer.

Our hypothesis is summarized as shown in the schematic figure (Fig. 10). Solar radiation recovers earlier in the stratosphere and the upper troposphere. With the polar sunrise, ozone depletion by catalytic reactions of chlorine cycle starts in the Antarctic stratosphere. Appearance of the ozone hole engenders UV enhancement and then production of atmospheric oxidants such as OH in the upper troposphere. Aerosol precursors with lower vapor pressure (e.g., H_2SO_4) are producible by photochemical oxidation. Also, NPF occurs already by end-August in the upper troposphere. As a consequence, NPF is enhanced in free troposphere under UV enhancement by O_3 hole during spring (end-August–November). Aerosol particles in fresh nucleation mode grow gradually by the condensation of condensable vapors in the free troposphere. Some aerosol particles in fresh and aged nucleation modes are transported to the lower troposphere in the Antarctic coasts. With condensation growth, some aerosol particles originated from spring NPF in the free troposphere can be grown to size greater than the critical diameter (ca. 50 nm) in the summer. Although NPF occurs in the boundary layer of the Antarctic coasts during summer, lesser aerosol particles derived from summer NPF in the boundary layer grow up to the critical diameter than from spring NPF in the free troposphere. Our results demonstrate that spring NPF plays an important role in aerosol population and cloud properties in the summer under conditions with appearance of the Antarctic ozone hole.

https://doi.org/10.5194/acp-2021-24
Preprint. Discussion started: 26 January 2021

Atmospheric Chemistry and Physics Discussions

4. Conclusion

Aerosol measurements were made using SMPS and OPC at Syowa Station, Antarctica in 2004–2006. Aerosol size distributions had mono-, bi-, tri- and quad-modal distributions during our measurements. The mono-modal distribution was dominant under strong wind conditions during May–August. The bi-modal distribution was identified through the year. Tri- and quad-modal distributions were observed mostly in September–April. Seasonal features of $N_{5\text{-}10}$ and J_5 imply that NPF identified at Syowa Station was associated with UV enhancement by ozone hole appearance in spring, maximum of solar radiation in summer, and minimum of sea-ice extent in February–March. Also, NPF occurs in free troposphere during spring and autumn and in the free troposphere and boundary layer during summer. Additionally, spring NPF and particle growth are linked to cloud properties during summer.

We obtained direct evidence indicating that spring UV enhancement by the ozone hole engendered spring NPF and growth in the Antarctic free troposphere. With recovery of the ozone hole (Solomon et al., 2016; Kuttippurath et al., 2017), aerosol properties and populations might be modified for the next several decades. As a result, indirect effects on atmospheric radiation budgets and climate change in the Antarctic regions during the summer can revert to their levels which prevailed before the ozone hole appearance. More aerosol measurements in Antarctic regions must be taken to monitor these trends and future effects.

Data availability

Data are available by contacting the corresponding author (KH: harakei@fukuoka-u.ac.jp).

Author contributions

KH, KO, and TY designed aerosol measurements at Syowa Station. KH, KO, and MY conducted wintering aerosol measurements at Syowa Station in 2004–2006. KH and CNH contributed to data analysis including SMPS/OPC data and meteorological data. KH prepared the manuscript and led data interpretation. All co-authors contributed to discussions about data interpretation and the manuscript.

Competing interests

The authors declare that they have no conflict of interest.

Acknowledgements

We thank the members of the 45th–47th Japanese Antarctic Research Expedition for assistance with aerosol measurements taken at Syowa Station. This study was supported financially by the “Observation project of global atmospheric change in the Antarctic” for JARE 43–47. This work was also supported by Grants-in Aid (No. 16253001, PI to T. Yamanouchi; No. 15310012, PI to K. Osada; and No. 22310013, PI to K. Hara) from the Ministry of Education, Culture, Sports, Science and Technology of Japan. The authors gratefully acknowledge the NOAA Air Resources Laboratory (ARL) for providing the HYSPLIT Transport and Dispersion Model and READY website used for this research (http://www.arl.noaa.gov/ready.html).

References

Asmi, A., Coen, C. M., Ogren, J., Andrews, E., Sheridan, P., Jefferson, A., Weingartner, E., Baltensperger, U., Bukowiecki, N., Lihavainen, H., Kivekäs, N., Asmi, E., Aalto, P., Kulmala, M., Wiedensohler, A., Birmili, W., Hamed, A., O’Dowd,

https://doi.org/10.5194/acp-2021-24
Preprint. Discussion started: 26 January 2021

C., Jennings, S., Weller, R., Flentje, H., Fjaeraa, A., Fiebig, M., Myhre, C., Hallar, A., Swietlicki, E., Kristensson, A. and Laj, P.: Aerosol decadal trends – Part 2: In-situ aerosol particle number concentrations at GAW and ACTRIS stations, *Atmospheric Chemistry and Physics*, 13, 895-916, doi:10.5194/acp-13-895-2013, 2013.

Bodhaine, B.A. Aerosol absorption measurements at Barrow, Mauna Loa and the South Pole. *Journal of Geophysical Research*: *Atmospheres*, **100**, 8967–8975 (1995).

Bromwich, D. H., Nicolas, J. P., Hines, K. M., Kay, J. E., Key, E. L., Lazzara, M. A., Lubin, D., McFarquhar, G. M., Gorodetskaya, I. V., Grosvenor, D. P., Lachlan-Cope, T., and van Lipzig, N. P.: Tropospheric clouds in Antarctica, *Reviews of Geophysics*, 50(1), doi:10.1029/2011RG000363, 2012.

Burrell, E., Kar, T. and Hansen, J. C.: Computational Study of the Thermodynamics of New Particle Formation Initiated by Complexes of H_2SO_4–H_2O–NH_x, CH_3SO_3H–H_2O–NH_x, and HO_2–H_2O–NH_x, *ACS Earth Space Chem.*, 3(8), 1415–1425, doi:10.1021/acsearthspacechem.9b00120, 2019.

Dall´Osto, M., Beddows, D. C. S., Tunved, P., Krejci, R., Ström, J., Hansson, H.-C., Yoon, Y. J., Park, K.-T., Becagli, S., Udisti, R., Onasch, T., O´Dowd, C. D., Simó, R., and Harrison, R. M.: Arctic sea ice melt leads to atmospheric new particle formation, *Scientific Reports*, 7(1), 3318, doi:10.1038/s41598-017-03328-1, 2017.

Fiebig, M., Hirdman, D., Lunder, C., Ogren, J., Solberg, S., Stohl, A., and Thompson, R.: Annual cycle of Antarctic baseline aerosol: controlled by photooxidation-limited aerosol formation, *Atmospheric Chemistry and Physics*, 14(6), 3083–3093, doi:10.5194/acp-14-3083-2014, 2014.

Gras, J. L. Condensation nucleus size distribution at Mawson, Antarctica: seasonal cycle. *Atmospheric Environment* **27**, 1417–1425 (1993).

Hara, K., Osada, K., Nishita-Hara, C., and Yamanouchi, T.: Seasonal variations and vertical features of aerosol particles in the Antarctic troposphere, *Atmospheric Chemistry and Physics*, 11, 5471-5484, doi:10.5194/acp-11-5471-2011, 2011a.

Hara, K., Osada, K., Nishita-Hara, C., Yabuki, M., Hayashi, M., Yamanouchi, T., Wada, M. and Shiobara, M.: Seasonal features of ultrafine particle volatility in the coastal Antarctic troposphere, *Atmospheric Chemistry and Physics*, 11, 9803-9812, doi:10.5194/acp-11-9803-2011, 2011b.

Hara, K., Osada, K., Yabuki, M., and Yamanouchi, T.: Seasonal variation of fractionated sea-salt particles on the Antarctic coast. *Geophys. Res. Lett*. **39**, L18801, doi:10.1029/2012GL052761, 2012.

Hara, K., Osada, K., Yabuki, M., Takashima, H., Theys, N., and Yamanouchi, T.: Important contributions of sea-salt aerosols to atmospheric bromine cycle in the Antarctic coasts, *Scientific Reports*, 8(1), 13852, doi:10.1038/s41598-018-32287-4, 2018.

Hara, K., Sudo, K., Ohnishi, T., Osada, K., Yabuki, M., Shiobara, M., and Yamanouchi, T.: Seasonal features and origins of carbonaceous aerosols at Syowa Station, coastal Antarctica, *Atmospheric Chemistry and Physics*, 19(11), 7817–7837, doi:10.5194/acp-19-7817-2019, 2019.

Hoppel, K., Bevilacqua, R., Canty, T., Salawitch, R., and Santee, M.: A measurement/model comparison of ozone photochemical loss in the Antarctic ozone hole using Polar Ozone and Aerosol Measurement observations and the Match technique. *Journal of Geophysical Research*: *Atmospheres*, **110**, D19304, doi:10.1029/2004JD005651(2005).

Humphries, R., Klekociuk, A., Schofield, R., Keywood, M., Ward, J. and Wilson, S.: Unexpectedly high ultrafine aerosol concentrations above East Antarctic sea ice, *Atmospheric Chemistry and Physics*, 16(4), doi:10.5194/acp-16-2185-2016, 2016.

Järvinen, E., Virkkula, A., Nieminen, T., Aalto, P., Asmi, E., Lanconelli, C., Busetto, M., Lupi, A., Schioppo, R., Vitale, V., Mazzola, M., Petäjä, T., Kerminen, -M V and Kulmala, M.: Seasonal cycle and modal structure of particle number size distribution at Dome C, Antarctica, *Atmospheric Chemistry and Physics*, **13**(15), 7473-7487, doi:10.5194/acp-13-7473-2013, 2013.

https://doi.org/10.5194/acp-2021-24
Preprint. Discussion started: 26 January 2021

Jen, C. N., Bachman, R., Zhao, J., McMurry, P. H. and Hanson, D. R.: Diamine-sulfuric acid reactions are a potent source of new particle formation, *Geophysical Research Letters*, 43(2), 867–873, doi:10.1002/2015gl066958, 2016.

Jones, A. and Wolff, E.: An analysis of the oxidation potential of the South Pole boundary layer and the influence of stratospheric ozone depletion. *Journal of Geophysical Research*, 108(D18), 4565, doi:10.1029/2003JD003379, 2003.

Kerminen, V.-M., Chen, X., Vakkari, V., Petäjä, T., Kulmala, M. and Bianchi, F.: Atmospheric new particle formation and growth: review of field observations, *Environmental Research Letters*, 13(10), 103003, doi:10.1088/1748-9326/aadf3c, 2018.

Kulmala, M., Kontkanen, J., Junninen, H., Lehtipalo, K., Manninen, H. E., Nieminen, T., Petäjä, T., Sipilä, M., Schobesberger, S., Rantala, P., Franchin, A., Jokinen, T., Järvinen, E., Äijälä, M., Kangasluoma, J., Hakala, J., Aalto, P. P., Paasonen, P., Mikkilä, J., Vanhanen, J., Aalto, J., Hakola, H., Makkonen, U., Ruuskanen, T., Mauldin, R. L., Duplissy, J., Vehkamäki, H., Bäck, J., Kortelainen, A., Riipinen, I., Kurtén, T., Johnston, M. V., Smith, J. N., Ehn, M., Mentel, T. F., Lehtinen, K. E., Laaksonen, A., Kerminen, V.-M. and Worsnop, D. R.: Direct Observations of Atmospheric Aerosol Nucleation, *Science*, 339(6122), 943–946, doi:10.1126/science.1227385, 2013.

Kulmala, M., Maso, M., Mäkelä, J., Pirjola, L., Väkevä, M., Aalto, P., Miikkulainen, P., Hämeri, K. and O'Dowd, C.: On the formation, growth and composition of nucleation mode particles, *Tellus Series B-chemical and Physical Meteorology*, doi:10.1034/j.1600-0889.2001.530411.x, 2001.

Kuttippurath, J. and Nair, P.: The signs of Antarctic ozone hole recovery, *Scientific Reports* **7**, 585, 2017.

Kyrö, M E, Kerminen, -M V, Virkkula, A., Maso, D. M., Parshintsev, J., Ruíz-Jimenez, J., Forsström, L., Manninen, H., Riekkola, -L M, Heinonen, P., and Kulmala, M.: Antarctic new particle formation from continental biogenic precursors, *Atmospheric Chemistry and Physics*, 13(7), 35273546, doi:10.5194/acp-13-3527-2013, 2013.

Matsumi, Y., Comes, F., Hancock, G., Hofzumahaus, A., Hynes, A., Kawasaki, M. and Ravishankara, A.: Quantum yields for production of $O(^1D)$ in the ultraviolet photolysis of ozone: Recommendation based on evaluation of laboratory data, Journal of Geophysical Research: Atmospheres (1984–2012), 107(D3), ACH 1-1-ACH 1-12, doi:10.1029/2001JD000510, 2002.

Matsumi, Y. and Kawasaki, M.: Photolysis of atmospheric ozone in the ultraviolet region, *Chem. Rev.* **103**, 4767–4782 (2003).

Millero, F., Feistel, R., Wright, D. and McDougall, T.: The composition of Standard Seawater and the definition of the Reference-Composition Salinity Scale. Deep Sea Research Part I: *Oceanographic Research Papers* **55**, 50–72 (2008).

Minikin, A., Legrand, M., Hall, J., Wagenbach, D., Kleefeld, C., Wolff, E., Pasteur, E., and Ducroz, F.: Sulfur-containing species (sulfate and methanesulfonate) in coastal Antarctic aerosol and precipitation, Journal of Geophysical Research, doi:10.1029/98jd00249, 1998.

Preunkert, S., Jourdain, B., Legrand, M., Udisti, R., Becagli, S., and Cerri, O.: Seasonality of sulfur species (dimethyl sulfide, sulfate, and methanesulfonate) in Antarctica: Inland versus coastal regions, Journal of Geophysical Research, 113(D15), doi:10.1029/2008jd009937, 2008.

Read, K., Lewis, A., Bauguitte, S., Rankin, A., Salmon, R., Wolff, E., Saiz-Lopez, A., Bloss, W., Heard, D., Lee, J. and Plane, J.: DMS and MSA measurements in the Antarctic Boundary Layer: impact of BrO on MSA production, Atmospheric Chemistry and Physics, 8(11), 2985-2997, doi:10.5194/acp-8-2985-2008, 2008.

Roscoe, H. K., Jones, A. E., Brough, N., Weller, R., Saiz-Lopez, A., Mahajan, A. S., Schoenhardt, A., Burrows, J. P. and Fleming, Z. L.: Particles and iodine compounds in coastal Antarctica, Journal of Geophysical Research: Atmospheres, 120(14), 7144–7156, doi:10.1002/2015jd023301, 2015.

https://doi.org/10.5194/acp-2021-24
Preprint. Discussion started: 26 January 2021

Shen, J., Xie, H.-B., Elm, J., Ma, F., Chen, J., and Vehkamäki, H.: Methanesulfonic Acid-driven New Particle Formation Enhanced by Monoethanolamine: A Computational Study, Environ. Sci. Technol., 53(24), 14387–14397, doi:10.1021/acs.est.9b05306, 2019.

Sipilä, M., Sarnela, N., Jokinen, T., Henschel, H., Junninen, H., Kontkanen, J., Richters, S., Kangasluoma, J., Franchin, A., Peräkylä, O., Rissanen, M. P., Ehn, M., Vehkamäki, H., Kurten, T., Berndt, T., Petäjä, T., Worsnop, D., Ceburnis, D., Kerminen, V.-M., Kulmala, M. and O'Dowd, C.: Molecular-scale evidence of aerosol particle formation via sequential addition of HIO3, Nature, 537(7621), 532–534, doi:10.1038/nature19314, 2016.

Solomon, S., Ivy, D. J., Kinnison, D., Mills, M. J., Neely, R. R., and Schmidt, A.: Emergence of healing in the Antarctic ozone layer, Science, 353(6296), 269–274, doi:10.1126/science.aae0061, 2016.

Weller, R., Minikin, A., Wagenbach, D. and Dreiling, V.: Characterization of the inter-annual, seasonal, and diurnal variations of condensation particle concentrations at Neumayer, Antarctica, Atmospheric Chemistry and Physics, 11(24), 13243-13257, doi:10.5194/acp-11-13243-2011, 2011.

Weller, R., Schmidt, K., Teinilä, K., and Hillamo, R. Natural new particle formation at the coastal Antarctic site Neumayer, *Atmospheric Chemistry and Physics* **15**, 11399–11410 (2015).

Yamanouchi, T. and Shudou, Y. Trends in cloud amount and radiative fluxes at Syowa Station, Antarctica. *Polar Science* **1**, 17–23 (2007).

Yu, H., McGraw, R. and Lee, S.-H.: Effects of amines on formation of sub-3 nm particles and their subsequent growth, Geophysical Research Letters, 39, doi:10.1029/2011gl050099, 2012.

https://doi.org/10.5194/acp-2021-24
Preprint. Discussion started: 26 January 2021

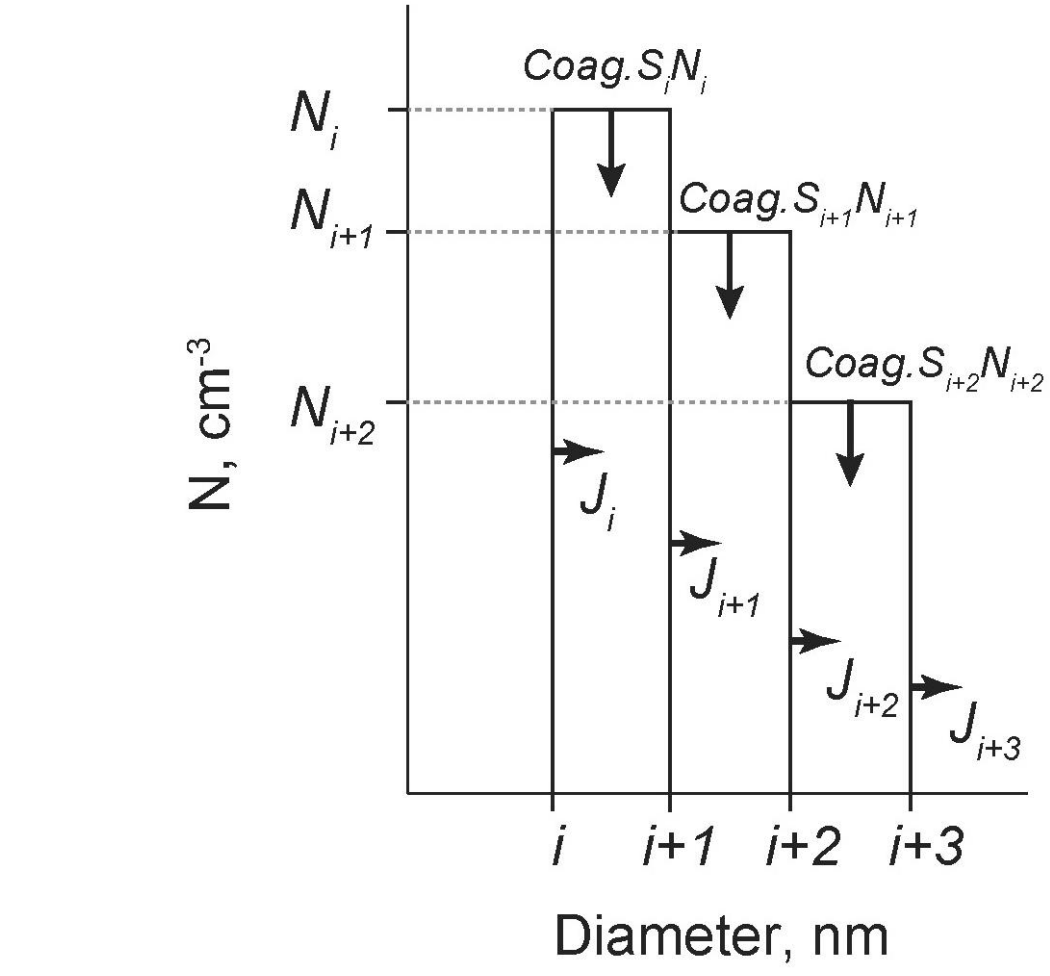

460

Figure 1: Schematic figure showing procedures used for the nucleation rate of aerosol particles with size of D_p = 5 nm (J_5). N_i, $Coag.S_i$, and J_i indicate the number concentrations, coagulation sink and growth (or formation) rate in each size bin.

https://doi.org/10.5194/acp-2021-24
Preprint. Discussion started: 26 January 2021

Atmospheric Chemistry and Physics Discussions

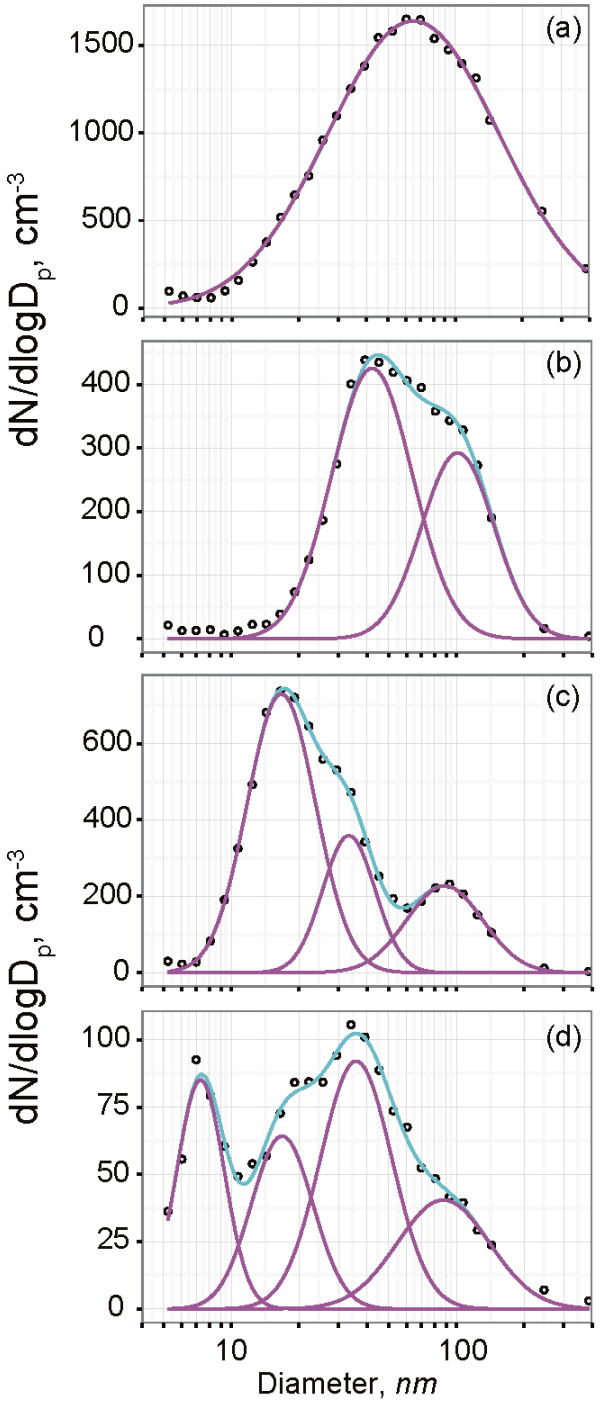

465 **Figure 2: Examples of aerosol size distributions with (a) mono-modal (3 May 2005), (b) bi-modal (4 March 2005), (c) tri-modal (14 February 2005), and (d) quad-modal (8 September 2006) structures. Circles, pink lines, and cyan lines in (a–d), respectively show the observed data by SMPS, the number concentrations in each mode by approximated by lognormal fitting, and total concentrations of the respective modes.**

https://doi.org/10.5194/acp-2021-24
Preprint. Discussion started: 26 January 2021

Atmospheric Chemistry and Physics Discussions

470

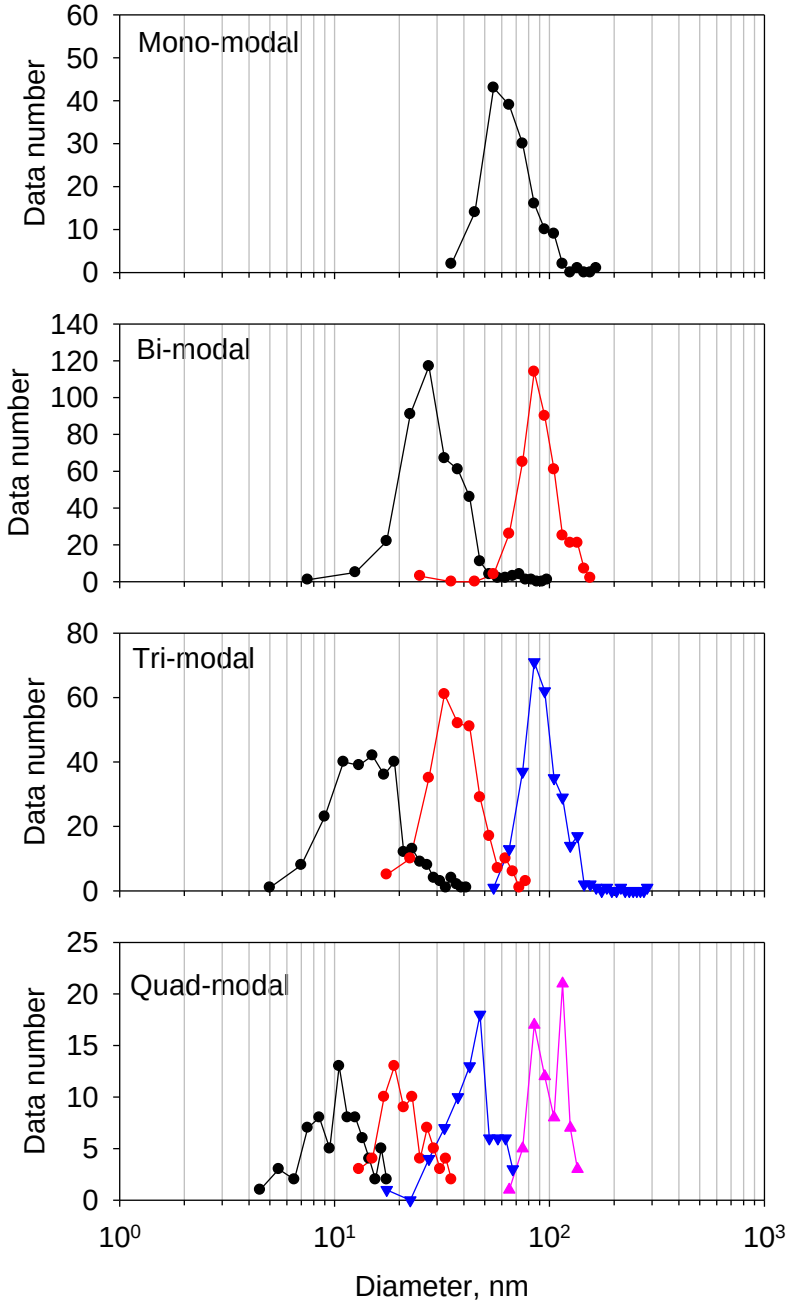

Figure 3: Histogram of modal sizes in each modal structure. Symbols and lines of black, red, blue, and magenta show histograms of 1st, 2nd, 3rd, and 4th modes in each modal strucutre.

https://doi.org/10.5194/acp-2021-24
Preprint. Discussion started: 26 January 2021

Atmospheric Chemistry and Physics Discussions

475

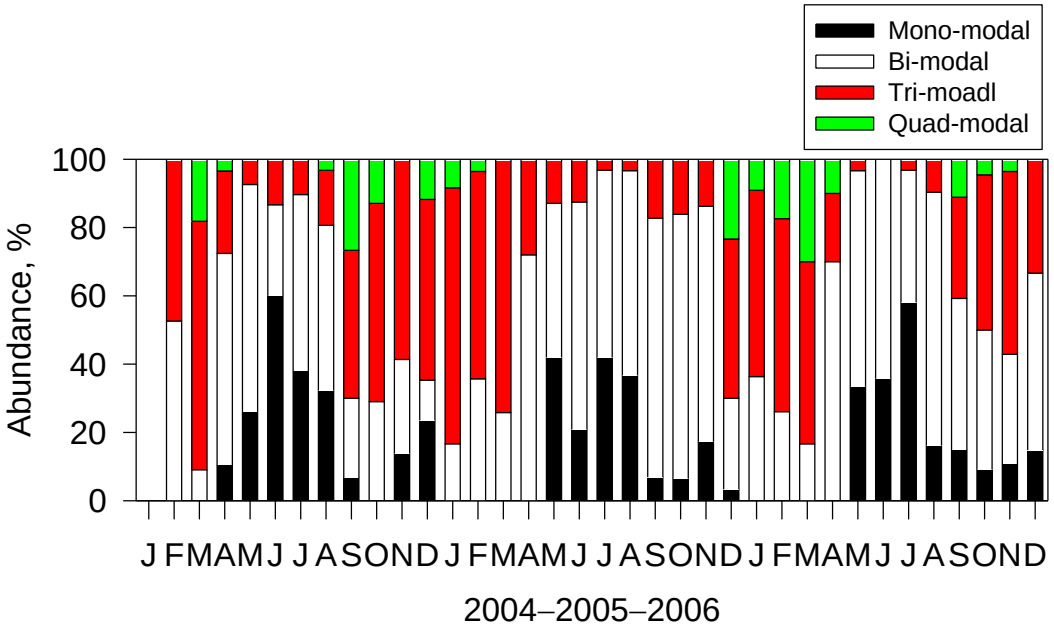

Figure 4: Seasonal feature of abundance of modal structure observed at Syowa Station, Antarctica.

https://doi.org/10.5194/acp-2021-24
Preprint. Discussion started: 26 January 2021

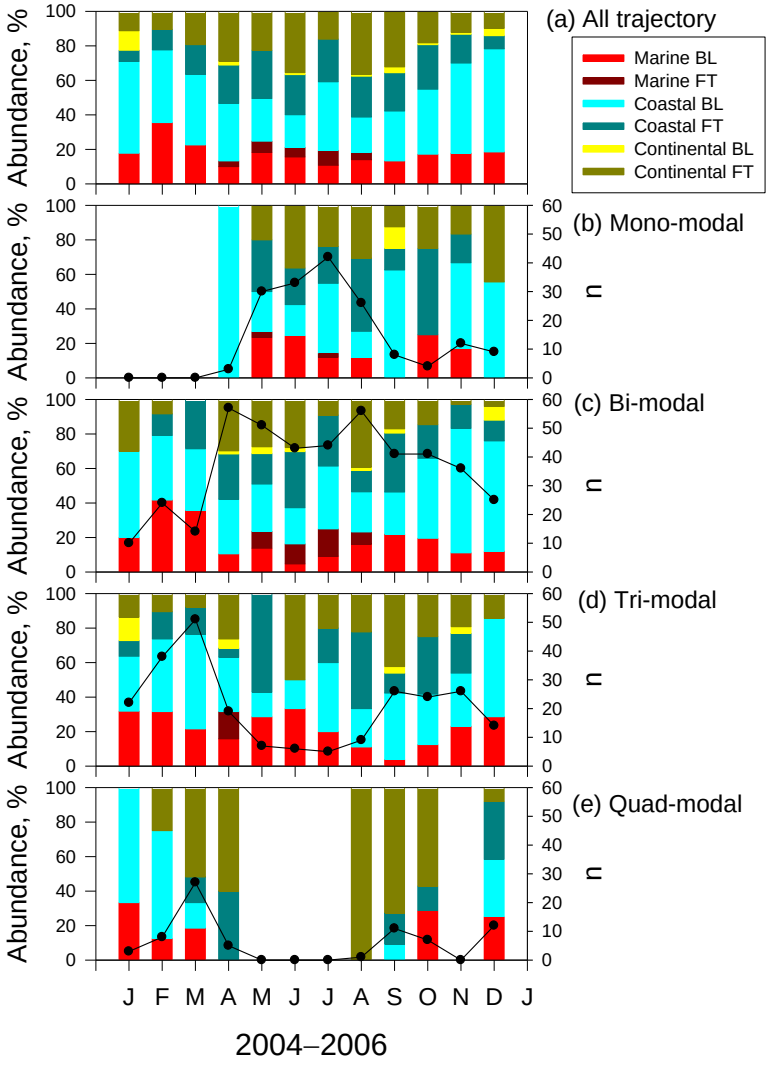

480

Figure 5: Seasonal feature of air mass origins of (a) all trajectory, (b) mono-modal structure, (c) bi-modal structure, (d) tri-modal structure, and (e) quad-modal structure at Syowa Station, Antarctica. "n" represents the number of the appearance of each modal structure.

https://doi.org/10.5194/acp-2021-24
Preprint. Discussion started: 26 January 2021

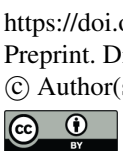

Atmospheric Chemistry and Physics Discussions

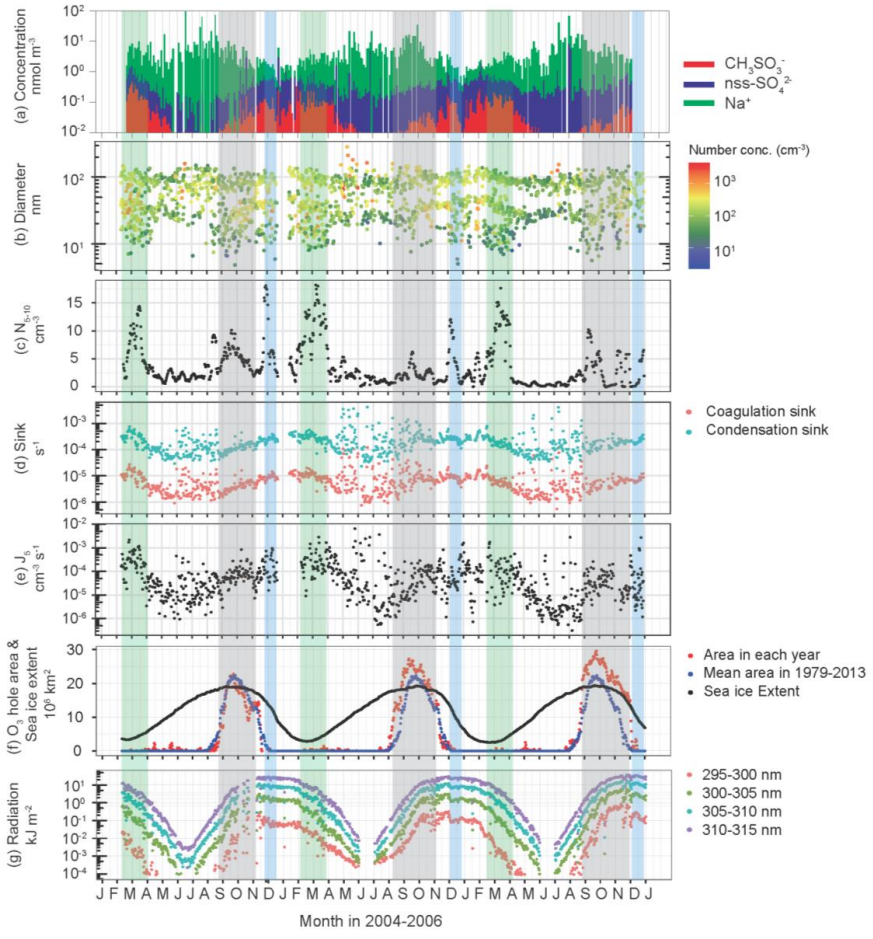

485

Figure 6: Seasonal variations of (a) the concentrations of $CH_3SO_3^-$, non-sea-salt (nss-) SO_4^{2-} and Na^+ in D_p <200 nm, (b) modal sizes and number concentrations in each mode, (c) 30-day running mean aerosol number concentrations of fresh nucleation mode (D_p = 5–10 nm), (d) coagulation sink of aerosol particle (D_p = 5nm) and condensation sink, (e) nucleation rate of aerosol particles with Dp = 5 nm (J_5), (f) extent of the Antarctic ozone hole, and (g) UV radiation near surface at Syowa Station, Antarctica during January 2004 – December 2006. Green-shaded, grey-shaded and blue-shaded bands respectively represent periods of minimum of sea-ice extent and high $CH_3SO_3^-$ concentrations, ozone hole appearance and summer solstice. Concentrations of nss-SO_4^{2-} were calculated using Na^+ concentrations and molar ratios in seawater (SO_4^{2-}/ Na^+ = 0.0602; Millero et al., 2008) during November–March and ratios in sea-salts (SO_4^{2-}/Na^+ = 0.01; Hara et al., 2012, 2018) in April–October because the SO_4^{2-}/Na^+ ratio is changed by sea-salt fractionation on sea-ice during April–October (Hara et al., 2012, 2018). The ozone hole extent and sea ice extent data were provided, respectively, by NASA (https://ozonewatch.gsfc.nasa.gov/) and the National Snow & Ice Data Center (https://nsidc.org/data/seaice_index). Daily mean UV data at Syowa Station were monitored by the Japanese Meteorological Agency (http://www.jma.go.jp/jma/index.html) using a Brewer spectrophotometer.

https://doi.org/10.5194/acp-2021-24
Preprint. Discussion started: 26 January 2021

Atmospheric Chemistry and Physics Discussions

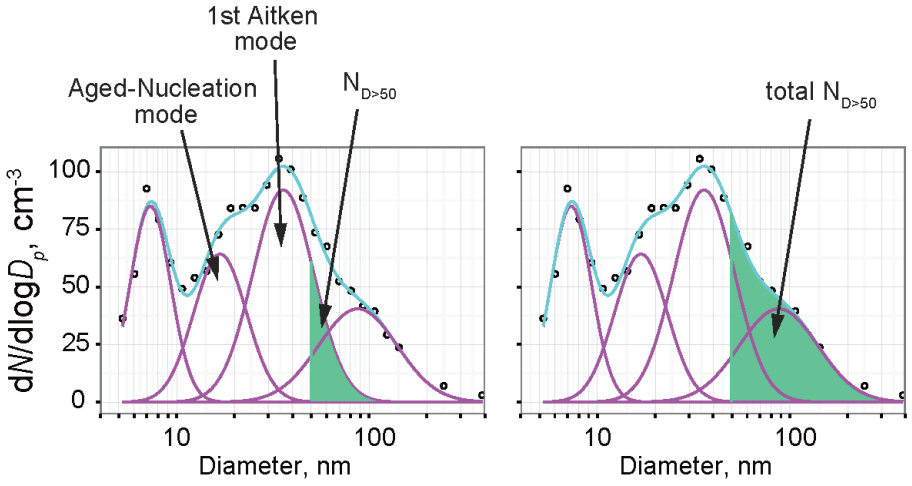

500

Figure 7: Schematic figure showing procedures used for R_{CCN} estimation. Circles, pink lines, and cyan lines respectively show the data observed using SMPS, the number concentrations in each mode by approximated by lognormal fitting, and total concentrations of each mode. Number concentrations of aerosols with size of D_p>50 nm in aged-nucleation mode and first Aitken mode ($N_{D>50}$) are given as shown for (a). Similarly, the total number concentrations of aerosols with size of D_p>50 nm (total-$N_{D>50}$) are given as shown for (b).

505

https://doi.org/10.5194/acp-2021-24
Preprint. Discussion started: 26 January 2021

Atmospheric Chemistry and Physics Discussions

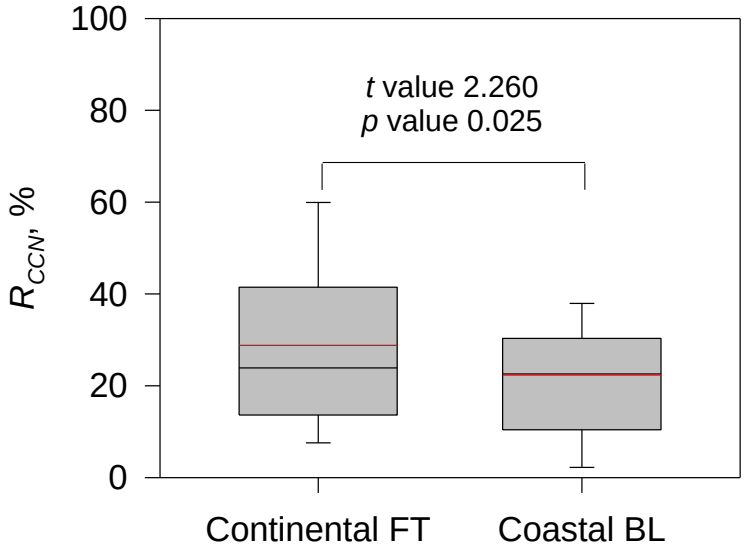

510 **Figure 8: Comparison of (a) R_{CCN} in the continental free troposphere (FT) and those in the coastal boundary layer (BL) during November – January in 2004–2006. *t* and *p* respectively denote *t*-values and *p*-values of *t*-tests. Degrees of freedom for the *t*-test were 155. Box plots show values of 90, 75, 50 (median), 25, and 10%, denoted respectively by the top bar, top box line, black middle box line, bottom box line, and bottom bar. Red lines show mean values.**

https://doi.org/10.5194/acp-2021-24
Preprint. Discussion started: 26 January 2021

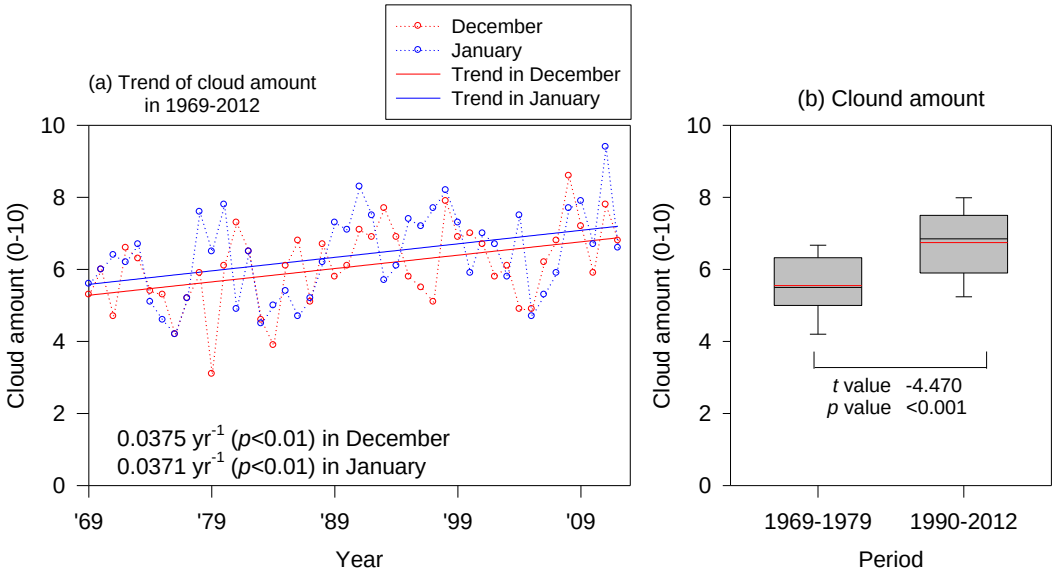

Figure 9(a) Trend of monthly mean cloud amount in 1969–2012 and (b) comparison of cloud amounts in December–January before and after appearance of the Antarctic ozone hole at Syowa Station, Antarctica. *t* and *p* respectively denote *t*-values and *p*-values of *t*-tests. Degrees of freedom for the *t*-test were 66. Because of the extended period of the ozone hole in 1980–1989, cloud amount data in the period were excluded from Fig. 9b. Box plots show values of 90, 75, 50 (median), 25, and 10% denoted respectively by the top bar, top box line, black middle box line, bottom box line, and bottom bar. Red lines show mean values. Cloud amounts were observed based on visual observations by the Japan Meteorological Agency (http://www.jma.go.jp/jma/index.html).

https://doi.org/10.5194/acp-2021-24
Preprint. Discussion started: 26 January 2021

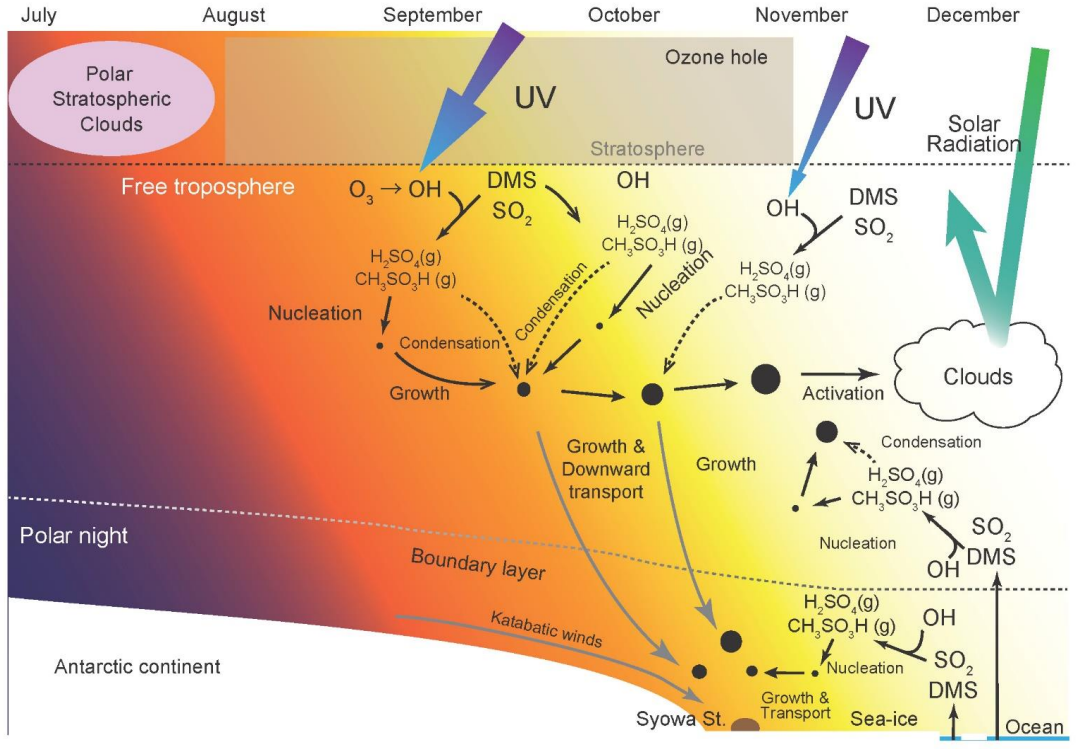

525

Figure 10: Schematic figure presenting our hypothesis.